Composite Structures 295 (2022) 115866

Contents lists available at ScienceDirect

Composite Structures

journal homepage: www.elsevier.com/locate/compstruct

In-Plane mechanical and failure responses of honeycombs with syntactic foam cell walls

Nicholas Pagliocca [a], George Youssef [b], Behrad Koohbor [a,c,*]

[a] Department of Mechanical Engineering, Rowan University, 201 Mullica Hill Rd., Glassboro, NJ 08028, USA
[b] Experimental Mechanics Laboratory, Department of Mechanical Engineering, San Diego State University, 5500 Campanile Drive, San Diego, CA, 92182, USA
[c] Advanced Materials & Manufacturing Institute, Rowan University, Glassboro, NJ 08028, USA

ARTICLE INFO

Keywords:
Architected Structures
Syntactic Foam
Honeycomb
Density Gradation
Digital Image Correlation

ABSTRACT

This work investigates the load-bearing and energy absorption capacities of hexagonal honeycombs with syntactic cell walls and spatial gradation of cell densities. Structures are processed and property-tuned by varying the volume fraction of hollow microspheres (microballoons), cell wall thickness, and spatial gradation of cell densities. The mechanical behavior of the structures is characterized by subjecting them to in-plane compression. Full-field deformation and failure responses of these structures at meso- and macro-scales are characterized by digital image correlation (DIC) and postmortem fracture analyses, respectively. Mesoscale analyses reveal heterogeneous strain accumulation at the cell hinges, which leads to a fracture in the vicinity of the hinge. Failure is characterized by a brittle mode in all samples. It is shown that the energy absorption capacity of the structures can be improved with the spatially-controlled incorporation of microballoons into the cell struts, at the penalty of reduced overall strength. In addition, cell-density gradation offers a notable improvement to the energy absorption performance over uniform density structures and a mechanism to lower structural density while achieving high mechanical performance.

1. Introduction

Architected structures have drawn notable attention in recent years due to their potential in offering tunable mechanical properties, achievable by altering their structures at the micro and meso scales. An example of such property-adjusted structures is honeycombs, in which the introduction of periodic cells with strategically adjusted unit cell geometries can lead to a wide range of desirable macroscopic properties. Some known structural benefits of honeycombs include improved impact energy absorption, reduced structural weight, and tailorable properties, such as the ability to introduce auxetic and structural anisotropic behaviors at various length scales [1–3]. Similar to periodic cellular structures, cellular composites and foams have offered attractive and viable design solutions in various research and industrial applications with improved and tunable responses [4–10]. A few applications of architected structural materials include civil and aerospace panels [11], automotive sandwich composites [4], soft robotics utilizing embedded intelligence [12], and honeycomb buffering sandwiches for packaging [13]. In most engineering applications, the need for lower density materials with adequate or improved mechanical load-bearing performance is essential.

Honeycombs are among the simplest classes of architected structures, whose mechanics and applications are well studied on theoretical and experimental grounds [14]. In general, the in-plane compressive response of honeycombs can be described with three deformation regions congruent with the mechanical behavior of other cellular solids. In low strain ranges, the structures exhibit linear elastic behavior, where the cell walls bend about the vertices of the cells, herein referred to as hinges. Once cellular collapse initiates, a plateau region develops and is exemplified in the stress–strain curve of the structure by near-constant stress until the opposing cell walls make contact. The latter process marks the onset of global densification and attributes to a rapid increase in the apparent stiffness of the structure. In the case of honeycombs fabricated from brittle base materials, cell walls bending about the hinges will fracture when the stresses exceed its modulus of rupture. In such cases, fragments may pack together upon further compression to display a similar phenomenon in the stress–strain curve as the plateau region [14,15], where confinement boundary conditions play a major role in the mechanical response.

Several investigators have studied the effects of cell strut thickness

* Corresponding author.
E-mail address: koohbor@rowan.edu (B. Koohbor).

https://doi.org/10.1016/j.compstruct.2022.115866
Received 23 December 2021; Received in revised form 20 May 2022; Accepted 1 June 2022
Available online 6 June 2022

and length on the overall load-bearing and energy absorption behaviors in honeycombs [14,16–18]. For instance, [17] studied the elastic behavior of honeycombs by building on the modeling approaches of [14]; the authors reported on the role of relative cell density in stiffness tuning and the impact of hinges in high cell density structures. [18] reported on the development of a beam model for thick-walled honeycombs with a uniform thickness and showed that stiffness is strongly coupled to the cell thickness-to-length ratio. Generally, the densification of honeycomb structures significantly decreases with increasing cell wall thickness. At the same time, an increase in the cell wall thickness leads to greater stiffness and higher load-bearing performance. Specifically, the stiffness of regular hexagonal honeycombs is proportional to t^3 (with t being the cell wall thickness), while the relative density is proportional to t [14,19]. Therefore, although primarily applicable to relatively small t/l ratios ($t/l < 0.25$, according to Gibson and Ashby [14]), an increase in the cell wall thickness, t, leads to a quadratic increase in the specific stiffness, *i.e.*, stiffness per unit density. In both modeling and optimization studies, cell geometry has also been explored to consider irregular cells and non-uniform wall thickness [20], structures with zero Poisson's ratio [21–23], and struts with curvature as they approach the hinge [24]. While direct tuning of cell geometry uniformly through the entire structure can offer some improvements, further optimization of the mechanical performance could be achieved by density gradation [25].

The design limits of tuning a uniform density can be expanded upon with *density gradation*. Cell density gradation in honeycombs can be achieved by varying cell geometry throughout the length of the sample [19,26]. The fundamental idea behind density gradation is to achieve high mechanical strengths and energy absorption by introducing layers with spatially variable cell geometry. The concept of density gradation extends not just to honeycombs but also foams. In the literature, many works experimentally investigate density-graded foams of various material classes, with some works considering quasi-static loading [27] and others considering impact conditions [9]. For instance, Ghimire and Chen [28,29] studied the fracture and failure of sandwich panels with multi-layered functionally graded foam cores. These works demonstrated the outperformance of a layered foam structure over homogeneous (single-layer) foam cores in enhancing the damage resilience and load-bearing capacity of sandwich panels fabricated from optimally graded foams. Exploring 2D architected materials, [26] characterized hyperelastic honeycombs manufactured using fused filament fabrication (FFF). It has been shown that controlled density gradients can significantly enhance energy absorption and damping performance over uniform cell density designs. [19] investigated the analytical optimization of honeycombs with discrete and continuous gradations for various gradients and found that density gradation in flexible hexagonal honeycombs improves energy absorption at the cost of structural stiffness. Several studies have also considered the energy absorption capability of graded honeycomb structures under dynamic loading conditions for regular and irregular graded structures, all reporting enhanced mechanical performance [30,31].

The introduction of self-similar structures inside cell struts has also offered new paradigms for improving the mechanical responses of architected structures. For instance, [32] studied the compressive response of hierarchical honeycombs and found improved post-yield crushing stress, plateau stability, strain-hardening, and improved energy absorption characteristics. In another study, [33] leveraged the improvements in mechanical response that self-similarity can offer in structures and extended them to the functional grading of hierarchical honeycombs. However, it is recognized that conventional manufacturing methods offer barriers to the practical production of such self-similar structures. On the other hand, additive manufacturing solutions have led to practical strategies for microstructural tailoring of materials in recent years [34], specifically valuable for printing cellular structures. Nonetheless, the continued development of cost-effective fabrication solutions is vital for industry realization of such printable, highly energy absorbent architected structures and is, thus, still a limitation.

An alternative approach to fabricating microstructure and architecture-controlled energy-absorbing structures has been the development of syntactic foams. Syntactic foams are porous composites in which hollow particles are embedded inside solid matrix material [10]. Syntactic foams are characterized by low density and tailorability, enhanced energy absorption, and load-bearing characteristics compared to single-phase (non-syntactic) foams [35]. The porous nature of syntactic foams yields a compressive response that mimics honeycombs, exemplifying linear elasticity, plateau, and densification regions [10,35–38]. In all aforementioned works, the microstructure of syntactic foams is reported to have a notable impact performance on the macroscale response of the structure. For instance, pioneering micromechanics modeling studies by Bardella and Genna [39,40] discuss the role of microballoons volume fraction on the deformation of syntactic foamed sandwiches in the linear elastic regime, highlighting the possibility of stiffness-to-weight optimization. Syntactic foams have been studied using several matrix materials, including polymers [10,41] and metals [36]. Afolabi *et al.* [42] provide a comprehensive review of manufacturing techniques for syntactic foams and an insight into the scope of researched matrix and filler materials that have been used in syntactic foams to date.

Novel composite structures can be developed by leveraging the attributes of honeycombs and syntactic foams discussed above, with improved energy absorption capacity and efficiency. To date, limited work has explored the so-called syntactic honeycomb structures. Among the limited work carried out on this topic is the research by Jhaver and Tippur [43], wherein the compressive behavior of aluminum-syntactic foam honeycombs was characterized. Syntactic honeycombs were developed by varying the volume fraction of hollow microspheres for in-plane loading along the length and width of the structure. It was found that a syntactic honeycomb can lead to improved stiffness and energy absorption. Zhang *et al.* [44] took a different approach by using a honeycomb structure as a reinforcing element in a syntactic foam matrix to study crack healing performance in the material. Researchers have also investigated the use of syntactic foams in honeycomb sandwich composites in dynamic and quasi-static loading conditions [45–47]. Lastly, syntactic foams with honeycomb-like structures have also been explored in the literature, *e.g.*, Yu *et al.* [48], where the authors investigated the use of novel manufacturing techniques to prepare the honeycomb-like syntactic foams.

In this work, we construct and characterize a novel composite honeycomb structure in which 1) the cell walls are composed of syntactic foams, and 2) density gradation is introduced through spatial gradation of the cell wall thickness in specific directions. Structures are realized by casting a mixture of an epoxy matrix embedding hollow ceramic microspheres (henceforth referred to as microballoons). We consider samples of uniform and graded cell densities with various volume fractions of the filler microballoons. In doing so, we demonstrate that the energy absorption and load-bearing performances can be simultaneously improved while the overall structural weight is reduced. Being the first work to investigate the combined effects of syntactic cell walls and density gradation, the main objective of the present study is to characterize the architected structures at the micro, meso, and macro scales and to report on their energy absorption and efficiency characteristics, as well as to understand the failure modes at large deformations.

2. Materials and methods

2.1. Honeycomb design

Uniform density and density-graded honeycombs were designed and fabricated with a microballoon filler material. In this work, we considered 0%, 10%, 20%, and 30% microballoon volume fractions. All uni-

form density honeycombs were designed with a constant cell edge size, l, of 5 mm and a depth, d, of 12 mm. The cell wall thickness, t, was varied to adjust density when needed. The relative density, ρ^*, of an isotropic thin-walled honeycomb (**Eq. (1)**) was used in describing the variation of density between samples [14].

$$\rho^* = \frac{2}{\sqrt{3}}\frac{t}{l} \tag{1}$$

Cell wall thicknesses of 1 mm, 2 mm, and 3 mm were considered for the uniform density structures. Uniform density structures are referred to as those with constant cell wall thickness. Single cells of the uniform density structures with representative filler material are illustrated in Fig. 1**A**.

Two discretely graded structures with 2-stage and 3-stage gradients were also considered in this work. The theoretical relative densities of the discretely graded structures were determined using **Eq. (2)** [19].

$$\rho^* = \frac{\sum_{i=1}^{N}\rho_i^* t_i}{\sum_{i=1}^{N} t_i} \tag{2}$$

where, ρ_i^* denotes the relative density of layer i, and t_i is the associated layer thickness. N represents the number of layers with uniform densities, taken to be 2 and 3 for the 2-stage and 3-stage graded structures, respectively. The 2-stage honeycomb was fabricated using 1 mm and 2 mm wall thickness gradations. The 3-stage structures were produced with 1 mm, 2 mm, and 3 mm wall thickness gradations. **Eq. (1)** and **Eq. (2)** are generally used for very thin-walled honeycombs ($t/l < 0.25$ [14]) and are employed here as estimates to characterize structural density when later discussing trends in mechanical responses. It is acknowledged that the validity of model predicted values is not guaranteed for samples with large wall thickness, *e.g.*, honeycombs with 3 mm cell wall thickness. Fig. 1**B** shows the design of structures with the 1 mm uniform honeycomb and the 2- and 3-stage graded honeycombs. Relative densities calculated for the samples are listed in Table 1.

2.2. Materials

The mechanical response of the cell wall materials and the microstructure of the microballoons were both characterized in-house. Samples were prepared by introducing proprietary ceramic microballoons (Fasco Epoxies, Inc., FL, USA) into a thermoset epoxy matrix (ProMarine Supplies Co., MI, USA). The nominal density of the microballoons was measured as 110 kg/m^3, and the nominal density of the matrix material was 1080 kg/m^3.

Table 1
Theoretical relative density of the examined structures.

	Uniform Density Structures			Density Graded Structures	
	Cell Wall Thickness, t			2-stage	3-stage
Microballoon volume fraction	1 mm	2 mm	3 mm		
0 vol%	0.23	0.46	0.69	0.36	0.59
10 vol%	0.21	0.42	0.63	0.34	0.46
20 vol%	0.19	0.38	0.57	0.30	0.42
30 vol%	0.17	0.34	0.51	0.27	0.37

The morphology and geometric features of the microballoons were characterized using scanning electron microscopy (SEM). Microballoons were uniformly deposited onto a carbon tape and examined using the scanning electron microscope (FEI Apreo 2). The mean diameter was determined as 44.9 ± 22.0 μm from the micrograph shown in Fig. 2**A**. To reveal and characterize the microballoons shell thickness, a small batch of microballoons was placed on carbon tape and subjected to pressure. The pressure was intentionally applied to crush some of the microballoons. Notably, these crushed microballoons were never used in any sample fabrications, *i.e.*, solely used for micrographic analysis purposes. Using the SEM image taken from the broken microballoons (Fig. 2**B**), the mean wall thickness was determined as 2.7 ± 0.8 μm. Histograms showing the distribution of the microballoons diameter and shell thickness are presented in Fig. 2**C and 2D**, respectively.

A careful examination of Fig. 2**A & 2B** reveals two observations. First, some small microballoons have fallen inside the larger crushed ones (see circled regions in Fig. 2**B**). This is substantiated based on a twofold rationale: 1) stiffness of smaller microballoons is greater than their larger counterparts, *i.e.*, higher pressure is required to crack the microballoons with smaller diameters, and 2) smaller microballoons tend to congregate around and between larger ones, allowing them to

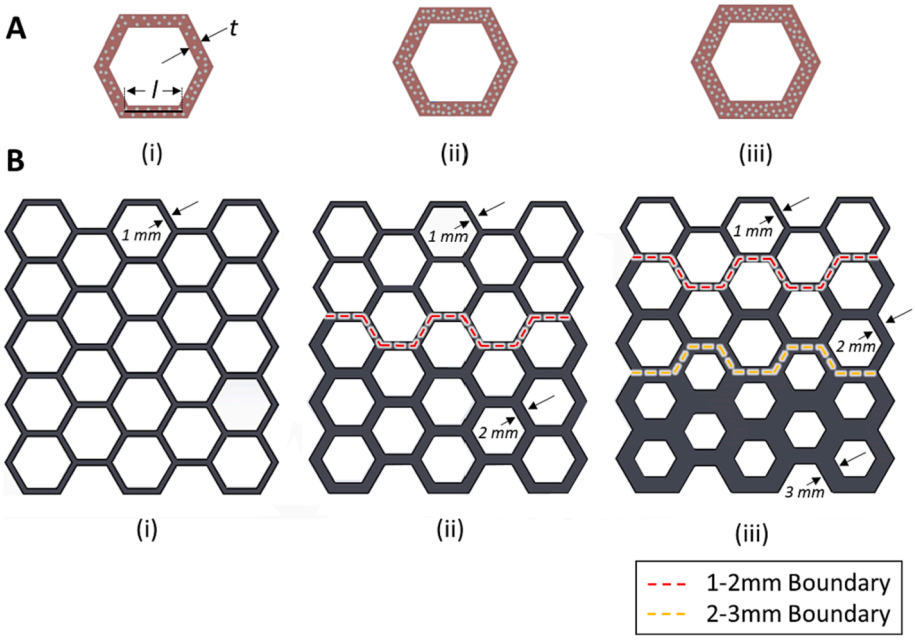

Fig. 1. Representative unit cell and structural design scheme: (A) Variation of the cell wall thicknesses for uniform density samples, wherein cell wall thickness, t, is (i) 1 mm, (ii) 2 mm, and (iii) 3 mm. Uniformly distributed filler material is shown schematically in each cell. (B) Schematics for (i) 1 mm uniform design, (ii) two-stage graded honeycomb, and (iii) three-stage graded honeycomb. Gradation boundaries are marked by dashed lines.

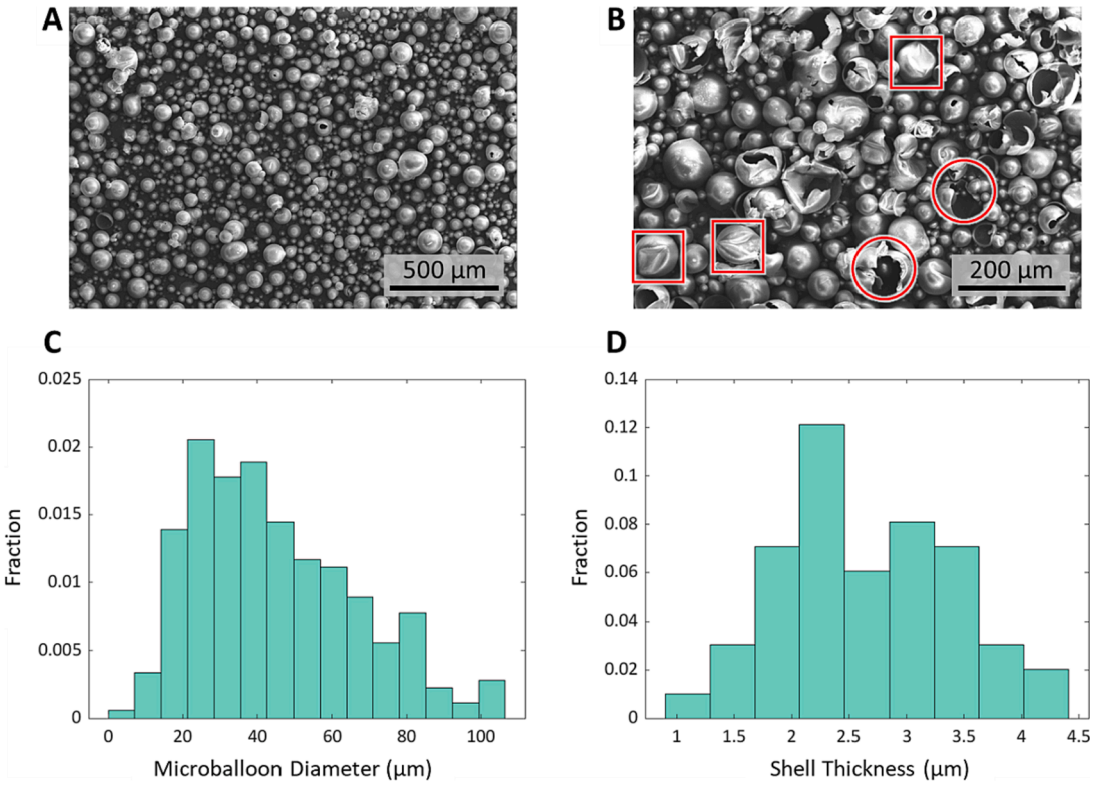

Fig. 2. Microstructural characteristics of the microballoons, showing (A) a SEM micrograph of the microballoons and (B) a micrograph of shattered microballoons used for the characterization of their average shell thickness. (C) and (D) show the diameter and shell thickness distribution of microballoons, respectively.

settle into the broken large microballoons. Second, some failed large microballoons exhibit ductile-like failure such as plastic deformation and wrinkles (see rectangular regions in Fig. 2**B**). This implies that local deformation heterogeneity may occur if the microballoons fail prior to or during sample fabrication. In general, microballoon failure did not occur when fabricating samples, as discussed later. Some shattered and wrinkled microballoons can also be seen in Fig. 2**A**.

The stress–strain behavior of the cell-wall (epoxy) material with various microballoon volume contents was characterized in tension and compression. Dog bone samples and compression cubes were cast using a custom mold under the same environmental conditions as the cast honeycomb structures. Dog bones were prepared with a gauge length of 100 mm, a width of 13 mm, and a thickness of 8 mm. Compression cubes were fabricated with 11 mm edge size. Tension and compression tests were performed under quasi-static conditions with 10 mm/min displacement rate on a Shimadzu test frame with a load cell capacity of 10 kN. All mechanical tests, including the aforementioned tests and those performed to characterize honeycomb structures (discussed in later sections), were performed several times to confirm repeatability. Experimental curves presented and discussed hereafter represent the average of the independent measurements that fall within a 95% confidence interval.

Fig. 3 shows the compressive stress–strain curves in the first quadrant and the tensile response in the third quadrant. Representative photographs of a 10 vol% microballoon dog bone and compression cube are shown in their respective regions of the stress–strain plot. The representation of compressive data in positive values in this figure is for consistency and ease of interpretation. Consistent with previous studies, [49,50] higher microballoon volume fractions led to an overall reduction in strength in tension and compression. Interestingly, the failure strain in compression improved by the introduction of microballoons compared to the terminal strain for the neat epoxy, *i.e.*, enhanced ductility, an observation that further justifies the use microballoons as a strategy to improve the energy absorption performance of honeycombs

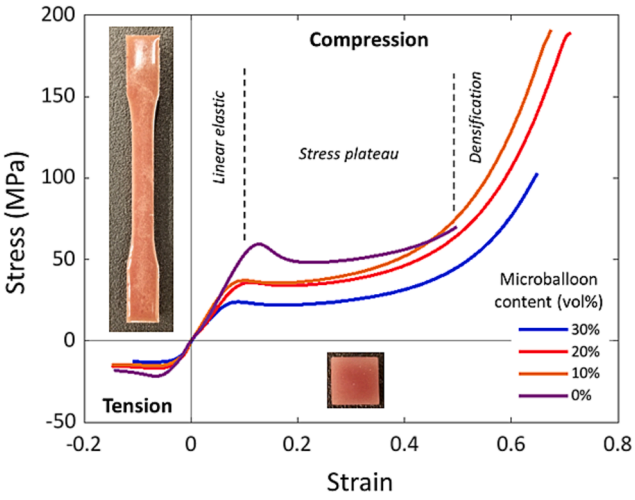

Fig. 3. Tensile and compressive stress–strain responses of the base epoxy with various microballoon volume fractions. Linear elastic, stress plateau, and densification regions are marked with vertical dashed lines on compression stress–strain curves. Representative dog bone and compression cube samples with 10 vol% are shown as insets.

[19]. The improvement in the compressive strain-to-failure was the highest for the syntactic structures with 20 vol% microballoon content. Despite an enhanced strain-to-failure, the introduction of microballoons had a negligible effect on the densification strain of the samples. For all samples, the onset densification strain was determined as the strain at maximum efficiency, described in detail in our previous works [8,19]. Accordingly, an onset densification strain of ~ 0.5 (in compression) was identified for all samples. In tension, a reduction in ultimate tensile strength and failure strain was observed for samples with various

microballoon contents. Data shown in Fig. 3 represents the average of three independent measurements for each condition. The mechanical properties of the epoxy with various microballoon contents were used to evaluate the primary failure modes at cellular scales. More information regarding the analytical failure analyses can be found in **Supplementary Information**.

Last but not least, density measurements were conducted for each *vol.*% sample set (see **Supplementary Information** for more details). A slight discrepancy was observed between the estimated densities the measurements performed on concurrently fabricated cubic coupon samples. These discrepancies likely account for the apparent large drop in plateau stress in the 30 vol% samples and the similarity of plateau stresses in the 10 and 20 vol% samples. Variation in density can be attributed to possible void content or the presence of some shattered microballoons during the fabrication process. Both are revisited later using a post-failure analysis.

2.3. Honeycomb fabrication and testing

Silicone rubber molds were designed for all the structures described in **Sec 2.1** to simultaneously cast four samples, one mold for each of the considered volume fractions. The material bed is elucidated in Fig. 4**A**. Negatives were fabricated using 3D printing and used for preparing the rubber molds. Microballoons were manually mixed with the epoxy for each volume fraction. The mixture was allowed ample time to gel before pouring into silicone rubber molds. The gelation process was required to make sure that the microballoons stayed suspended in the mixture during the curing time. Cast samples were allowed to cure for five days in a fume hood prior to removal from the mold and testing. The methods used for sample preparation are intended to be easily replicable for real-world applications. While not used in this work, we should emphasize that treating the filler materials with specific chemical/sizing agents can lead to higher microballoon-epoxy interface strength. A 2 mm uniform density structure with 20 vol% microballoon and a 3-stage graded structure with the same overall volume fractions are shown in Fig. 4**B & 4C** for reference.

Cast samples for all volume fractions and gradations were tested in quasi-static compression. A multiscale 2D DIC setup was utilized to characterize the meso- and macro-scale deformations of the samples simultaneously. Macroscale observations were conducted to enable a visual comparison of the macroscale deformation and failure of the samples. In addition, mesoscale measurements were carried out to provide quantitative evidence on the possible deformation and failure mechanisms, as discussed in the forthcoming sections.

The multiscale image-based characterization approach was facilitated through the design of a dual-camera setup. The schematic of the multiscale mechanical characterization approach and a photograph of the actual experimental setup are shown in Fig. 4**D & 4E**, respectively. The mesoscale region of interest is also marked in Fig. 4**B** for clarity. Prior to testing, a monochromatic high contrast speckle pattern was applied on the front (camera facing) surface of each sample using spray paint. Mechanical tests were performed immediately after pattern application to avoid paint flaking due to the forecasted large deformations. The compressive load was applied at a constant rate of 10 mm/min until failure. Imaging (for deformation observation and DIC analysis purposes) and load data acquisition were synchronized and performed at a rate of 1 Hz. Images acquired during mechanical tests were analyzed in the commercially available DIC software Vic-2D (Correlated Solutions, Inc., SC, USA). Mesoscale DIC analyses were performed using 15 pixels (500 μm) subset and 4 pixels (133 μm) step sizes.

Specific energy absorption, W, (*i.e.*, energy absorption per unit volume) characteristics of each sample were quantified by determining the area under the stress–strain curve, as expressed in **Eq. (3)** [19,51]. In addition, the efficiency parameter, η, defined as the ratio of absorbed energy to the current stress, **Eq. (4)**, was also determined for each sample configuration.

$$W(\varepsilon) = \int_0^{\varepsilon} \sigma . d\varepsilon \tag{3}$$

$$\eta(\varepsilon) = \frac{\int_0^{\varepsilon} \sigma . d\varepsilon}{\sigma} \tag{4}$$

The efficiency parameter introduced in **Eq. (4)** is used to determine

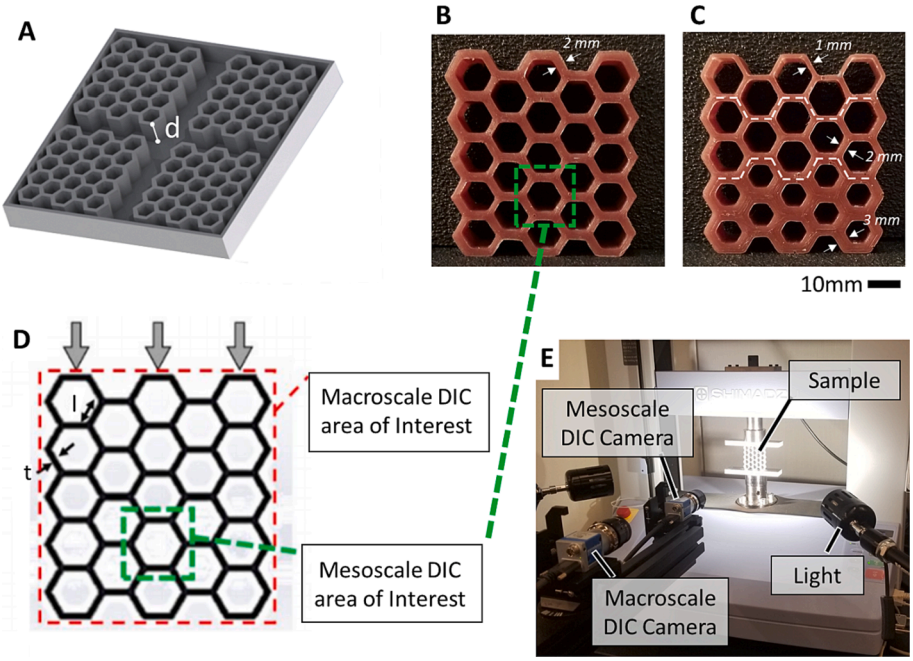

Fig. 4. (A) Material bed negative designed for the casting process. The depth, d, was 12 mm for all structures examined herein. (B) Uniform density ($t = 2$ mm) 20 vol %, and (C) 3-stage graded 20 vol% samples, prior to testing. (D) Schematic of a uniform density sample with macro and mesoscale DIC areas of interest marked with red and green dashed rectangles, respectively. (E) The dual-camera experimental setup used for multiscale DIC analyses.

the densification strain and a quantitative measure for the energy absorption response of the structures. Accordingly, the global densification strain can be identified as the strain associated with maximum efficiency [19]. In **Eqs. (3) and (4)**, σ and ε symbolize the global stress and strain. In the present work, stress, σ, is defined by the ratio of the compressive load, P, to the undeformed rectangular cross-sectional area of the homogenized equivalent structure. We take the total width (all five cells across, as shown in Fig. 1**B**) and a depth, d, of 12 mm, as shown in Fig. 4**A** for the undeformed cross-sectional areas in all analyses. The ratio between the change in sample height and its initial height is used to define strain, ε, in all cases.

3. Results and discussions

3.1. Mechanical response of uniform structures

Fig. 5**A** shows the compressive stress–strain responses of the uniform density structures described in **Sec 2.1** with 0 vol%, 10 vol%, and 20 vol % microballoon. The 1 mm and 2 mm structures show a slight delay in global densification and a reduction in overall strength between the 0% and 10% volume fraction samples. This reduction in the overall strength is reasonable because the overall mechanical strength of the base material has deteriorated after introducing the microballoons (see Fig. 3). The densification strain significantly decreases for all investigated volume fractions as the cell wall thickness increases. At the same time, and as anticipated, an increase in the cell wall thickness leads to higher stiffness and strength, exemplified by the apparent increase in the elastic modulus (initial slope of the curve) and yield stress. This observation agrees with the existing literature on the role of cell density on the mechanical response of hexagonal honeycombs [14,19] and is further discussed in **Supplementary Information**. It should be noted that the samples with microballoon volume fraction $>$ 20% failed before a stress plateau, thus showing no discernible densification. Failure for those samples was observed in the form of brittle fracture initiated in the vicinity of the cell hinges, consistent with the background studies discussed in the introduction. For brevity and their extremely low ductility and inferior energy absorption capacities, results obtained for these higher volume fraction structures are excluded from Fig. 5**A** but provided as **Supplementary Information**.

The energy absorption capacity of the structures is illustrated in Fig. 5**B**. Syntactic structures show energy offset from the neat structures (0 vol% microballoon), with lower specific energies at small strains. Thicker cell walls correspond with higher energy absorption and stiffness at lower strains. Fig. 5**C** shows the energy absorption efficiency of the structures with 0% and 10% microballoon volume contents. The introduction of the microballoons is shown to improve the efficiency response of the 1 mm and 2 mm structures, particularly at strains $<$ 0.4. The same trend is also observed for the 20 vol% samples at strains below 0.2. Note that due to the early development of failure in the 20 vol% samples, efficiency results could not be determined for larger strain conditions.

Spikes observed in the efficiency curves indicate collapsing cell walls in the structure. As such, observation of multiple spikes in the efficiency curves for 2 mm wall thickness samples indicates the sequential collapse of the cell walls in response to the compressive load. Another important point worth mentioning is that in cases where multiple efficiency spikes are observed, the final spike represents the onset of global densifications, *i.e.*, the points where the structure saturates its energy absorption performance [19]. In other words, the final efficiency peak is a practical indicator of the global densification strain in the structure. Interestingly, the strains associated with the final efficiency spike in the 2 mm cell wall samples coincide at $\varepsilon = 0.6$. This observation implies that in spite of a reduction in density (see Table 1), the incorporation of 10 vol% microballoons in the 2 mm samples leads to no particular improvement in the densification onset strain. On the other hand, the same comparison made for structures with 1 mm cell wall thickness shows a slight increase in the densification onset strain when the microballoon content is increased from 0 vol% to 10 vol% (Fig. 5**D**). Although relatively small,

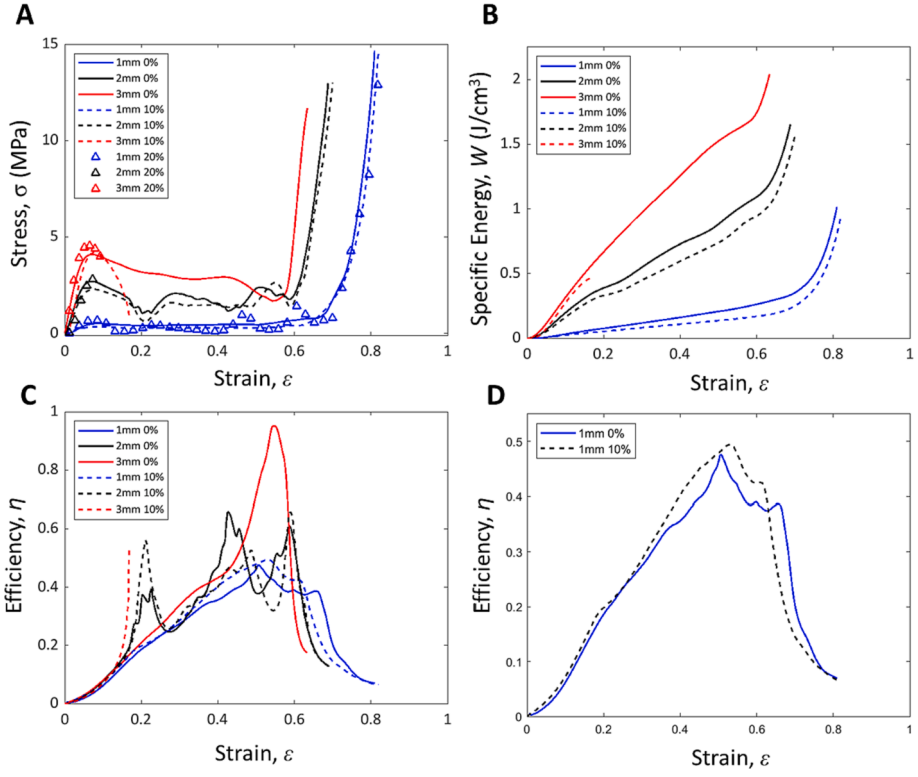

Fig. 5. Uniform (single stage) density sample analysis showing: (A) stress–strain curves, (B) specific energy-strain, and (C) efficiency-strain plots. A comparison of the efficiency-strain data obtained for the 1 mm structure with 0 vol% and 10 vol% microballoon loading is shown in (D).

the positive improvements in densification strain and energy absorption efficiency and the reduction in relative density for the 10% microballoon content is promising.

3.2. Mechanical response of graded structures

The compressive stress–strain response of the graded structures is illustrated in Fig. 6**A**. For comparison, this plot also shows the stress–-strain curve of the uniform structure with 1 mm cell wall thickness. Regardless of the microballoon volume content, the 2-stage and 3-stage structures show a clear improvement in the load-bearing performance. The pseudo-step-wise increase in the stress–strain responses of the graded (2-stage and 3-stage) structures is typical of density-graded honeycombs and is attributed to the sequential deformation and collapse of layers with various relative densities [19,26]. Consistent with the observations discussed in **Sec. 3.1**, the addition of a 10% microballoons volume fraction to the structures has led to an overall decrease in strength; such strength reductions are more pronounced in the case of the 3-stage structures. The latter observation is most likely associated with the more substantial weakening of the thicker (*i.e.*, 3 mm) cell walls in the 3-stage structure that led to premature failure and, thus, deteriorated the overall load-bearing behavior of the structure. Nonetheless, comparing the stress–strain response of the uniform (Fig. 5**A**) and density-graded structures indicates an improvement in the load-bearing capacity of the structure by density gradation, especially at high strains.

The enhanced load-bearing behavior is also manifested in the energy absorption capacity of the graded structures, shown in Fig. 6**B**. Considering energy absorption of the structures, the 3-stage graded structure shows a ~ 1 J/cm^3 improvement in the peak energy absorption when compared to the 3 mm cell wall thickness samples with uniform density. This 1 J/cm^3 increase is equivalent to an approximate 50% improvement in energy absorption. The significance of such enhancement becomes even more evident by comparing the relative density of the 3 mm uniform density structures with that of the 3-stage graded ones. Similar comparisons can be made for the 2-stage structures. While results are less pronounced for the 2-stage designs, the density reduction in the 2-stage structure compared to its 2 mm uniform counterpart could still be appealing in real-world applications.

Mass-specific properties for the stiffness, the first stress plateau, and energy absorption are characterized for all 0 vol% and 10 vol% structures and included in the **Supplementary Information** for brevity. The incorporation of microballoons leads to an overall reduction in mass-specific elastic modulus and plateau stress in most sample sets, which is consistent with the results reported in Fig. 3, Fig. 5, and Fig. 6. The reduction in elastic modulus and plateau stress is small but most pronounced with the 3-stage structures. Consistent with results from Fig. 5 and Fig. 6, the offset in densification strain can slightly improve in specific energy properties. The improvement is most pronounced in the 2-stage graded structures, while others perform roughly the same as the 0 vol% samples of their respective sample set. The latter observation validates that the syntactic structures perform comparably or even better than neat epoxy structures without compromising their structural integrity. The small variations in the response of the specific properties indicate that cell density and the cell density distribution dominate over the role of the filler material for low volume fractions. This can be directly observed when comparing the mechanical behaviors of 0 vol% and 10 vol% structures, which often showed similar responses,

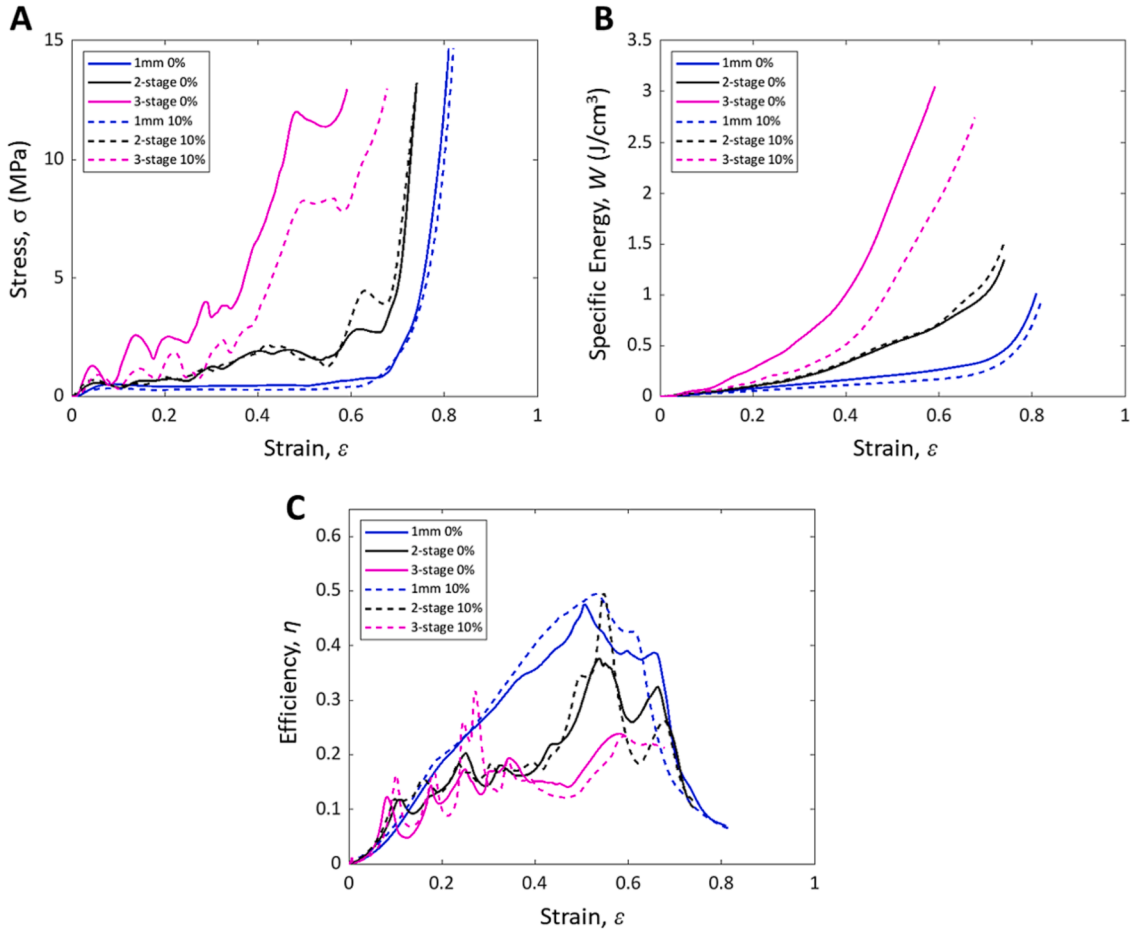

Fig. 6. Mechanical test results for density-graded structures showing: (A) stress–strain, (B) specific energy-strain, and (C) efficiency-strain curves.

excluding the 3-stage graded structure. The significant shift in stress–-strain response is attributed to the plateau and densification of the 1 mm layer, which happens significantly earlier in this structure than all the others. Other filler materials may encourage greater influence from the syntactic cell walls on the specific material property responses.

The efficiency response for the graded structures is shown in Fig. 6**C**. Again, the efficiency curves for 1 mm wall thickness uniform density (with 0 vol% and 10 vol% microballoon contents) are included in this graph for comparison. The 2-stage structures with 0 vol% and 10 vol% microballoons show higher efficiencies than the 3-stage samples. In addition, the 2-stage structures also show efficiency peaks at strains $>$ 0.65. The improvements in both energy absorption efficiency and global densification strain for the 2-stage samples are essential characteristics that highlight the positive contribution of density gradation in the simultaneous improvement of the load-bearing and energy absorption capacities. Comparing the load-bearing and energy absorption metrics obtained for both uniform and graded structures with various microballoon loading suggests that a 2-stage gradation with 10 vol% microballoon may be an optimal design within the range of samples examined in this work.

3.3. Multiscale DIC and failure analyses

Image correlation analyses were conducted to study the full-field deformation response of the samples at macro- and *meso*-scales. An emphasis is afforded to the deformation of the 2-stage 10 vol% structures, considering their overall improved performance when compared with other samples. For comparison, the results of the 2-stage 10 vol% structure are contrasted with those of the uniform density structure with a 1 mm cell wall thickness and the same 10% microballoon content.

The macroscopic deformation behavior of the 2-stage 10 vol% structure is shown in Fig. 7**A**. The macroscale deformation of this sample is exemplified by a progressive compression and failure of the top cell rows of the structure, *i.e.*, the cell rows whose wall thicknesses are 1 mm. The progressive deformation propagates into thicker cell rows at strains $>$ 0.25. This transition marks the onset of the deformation in thick cell wall sections in the structure. The step-wise yielding and stress plateaus discussed earlier in Fig. 6**A** are associated with sequential deformation and failure progression in the 2-stage graded structure.

Compared with the step-wise compression response of the 2-stage sample, deformation of the 1 mm 10 vol% uniform density structure (Fig. 7**B**) occurs in a uniform manner wherein all hexagonal cells in the structure start to deform upon the application of the compressive load. In this case, cells continue to bend uniformly about their hinges until the onset of global densification. A direct comparison of the energy absorption against strain for the structures presented in Fig. 7 can be found in Fig. 6**B,** where the superior energy absorption of the 2-stage structure is quantified.

In all examined samples, fracture occurred near the cell hinges. Nonetheless, the strains associated with sample failure differed and depended on the thickness and microballoon content in cell walls. The local deformation at the cell hinge vicinities depends on the thickness and microballoon volume content. The correlations between mesoscale instability and thickness have been highlighted in previous studies. In particular, it has been shown that increasing the cell wall thickness to edge ratio can lead to a transition from elastic buckling to brittle fracture in hexagonal honeycombs [52]. The dominance of brittle failure in the samples examined in this work has been discussed in **Supplementary Information**. Considering the comparably improved load-bearing and energy absorption responses of the 2-stage 10 vol% samples, mesoscale DIC analyses were performed to understand better the underlying mechanisms that may have led to the outperformance of this sample compared with others.

The evolution of the in-plane strain components for the 2 mm 10 vol % structure at various global strains is shown in Fig. 8. At small global strains reported in Fig. 8, the shear strain, ε_{xy}, is notably lower in magnitude than the axial, ε_{yy}, and transverse, ε_{xx}, strains. At larger global deformations, the relative scale of shear strain increases. However, the axial and transverse strains remain dominant over the shear strain. The axial and transverse strain components show heterogeneous distributions with high strain concentrations occurring at the cell hinges. The locations of these high strain regions shift towards the center of the cell struts at larger deformations. The expansion of these strain zones along the cells before complete failure attributes to the rotation of the cell struts, reflected at larger scales by noticeably larger macroscopic strains to failure. The concentration of local axial and transverse strains near the cell hinges possibly leads to the failure of microballoons within these regions, ultimately resulting in a semi-brittle failure mode in the cell hinge vicinity.

High magnification post-fracture images are shown in Fig. 9 for the neat and syntactic foam samples. Observations from the mesoscale DIC analyses suggested that the accumulation of high strain regions at the cell hinges may be a primary instigator for structural failure. Examining the 0 vol% sample shown in Fig. 9**A**, the cell struts are shown to have failed in a brittle mode. The brittle failure in this case is characterized by clean cleavage fractured planes that are common to many thermoset polymers [53]. Fig. 9**B & 9C** show images taken from 2 mm and 1 mm cell struts with 10% microballoon volume fraction, respectively. Examination of these syntactic honeycomb samples reveals a rough fracture surface. This observation indicates that the microballoons encompassed within the syntactic cell walls likely break at low strains and lead to an instantaneous reduction in the load-bearing sections of the cell struts. This phenomenon then leads to the fracture of the epoxy embedding the microballoons. Local deformation and failure behaviors of the hinges are also characterized by the increased porosity near the fracture surfaces.

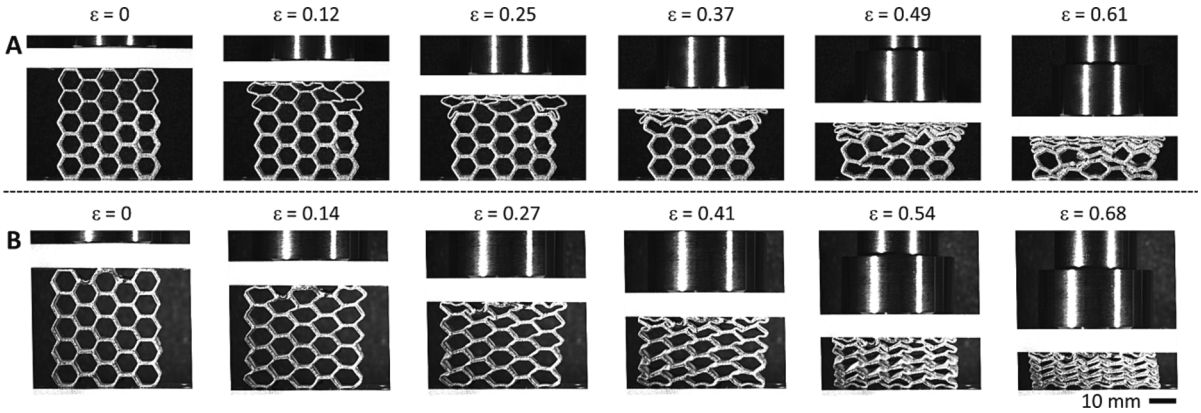

Fig. 7. Macroscale deformation of (A) the 2-stage, and (B) uniform density structure with 1 mm cell walls. Both samples have 10% microballoon volume content.

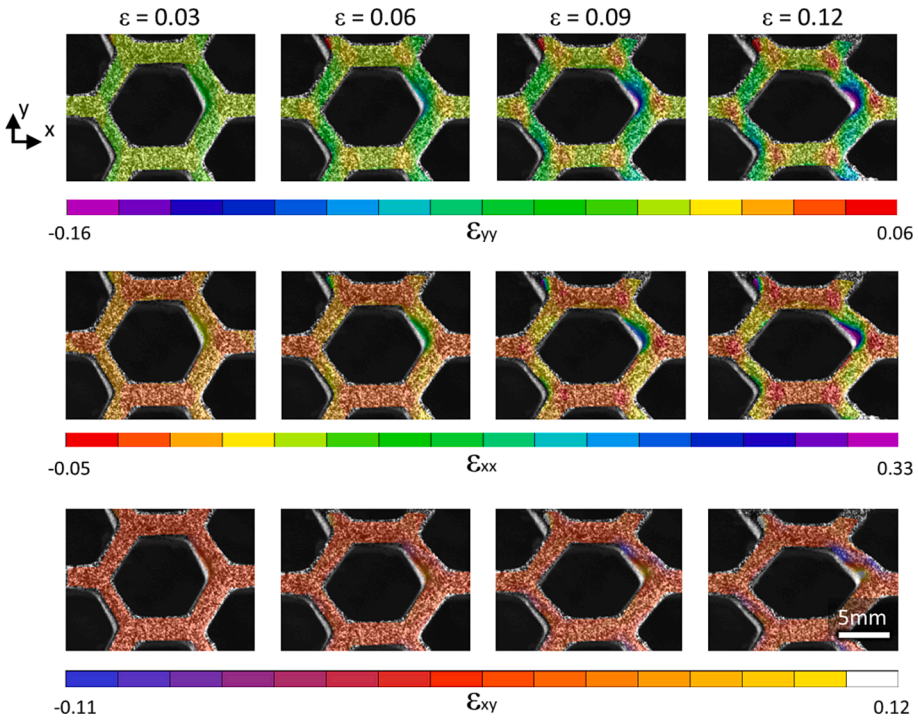

Fig. 8. Mesoscale DIC analysis of the 2 mm 10 vol% sample showing the evolution of the in-plane strain components, ε_{yy}, ε_{xx}, and ε_{xy}.

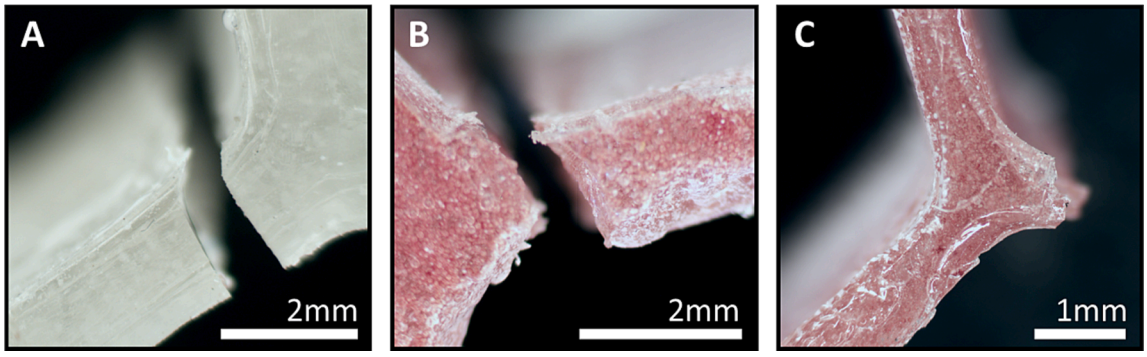

Fig. 9. High magnification optical images showing the fracture zone and morphology in (A) 2 mm uniform density sample with 0 vol% microballoon content, (B) 2 mm 10 vol% structure, and (C) 1 mm 10 vol% uniform density structure.

It is also important to address microstructural defects that may expedite crack initiation and propagation in the structures. Reported differences in the theoretical and experimental densities (provided as **Supplementary Information**) indicate the possible presence of some void content. It is known that void spaces in particle reinforced composites can lead to early material failure. For example, in studying the role of microballoon volume fraction, [49] found that increased volume fractions in syntactic materials can lead to material failure at early deformation stages due to the detrimental role of the particles serving as stress concentration zones. Moreover, the relative difference between the elastic moduli of the matrix and filler material (as attributes to the load partitioning between the two constituents) may even have a more prominent effect leading to stress concentration and premature failure [54]. In the case of syntactic honeycomb structures, the concurrent effects of increased volume fraction and relatively large stiffness difference between the ceramic microballoons and the epoxy matrix (although not quantified herein) can be superimposed on the already elevated stress state near cell hinges, eventually leading to semi-brittle failure in the vicinity of cell hinges.

The microscale failure in samples is further studied by SEM analysis

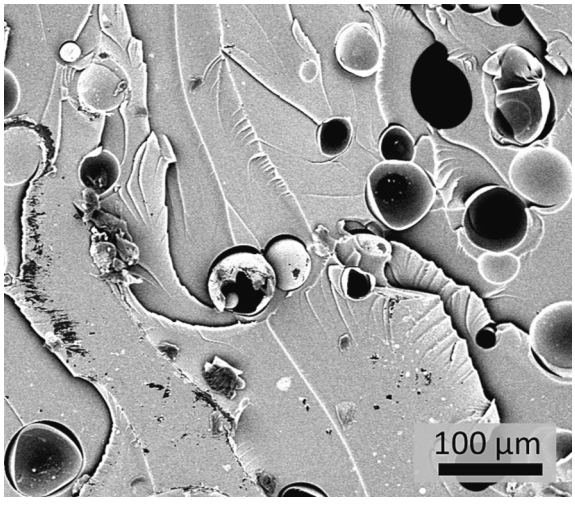

Fig. 10. SEM micrograph of the fracture surface of the 2 mm 10 vol% structure.

of the fracture surfaces. Fig. 10 shows a representative fracture surface of the 2 mm 10 vol% sample shown earlier in Fig. 8 and Fig. 9. The fracture surface examination elucidates that microballoons are well bonded to the matrix material, minimizing the void space between the constituent materials. The latter argument is justified by the preservation of areas where particles were dislodged during mechanical testing and failure. Nonetheless, some void space is expected given the small difference between theoretically determined and experimentally measured densities. Another interesting feature observed in Fig. 10 is the wrinkling of some of the microballoons, consistent with the results shown earlier in Fig. 2**B**. In addition, the textured fracture surface morphology of the epoxy with evident contortions around the microballoons emphasizes the possible role of microballoons as stress/strain concentration sites, leading to increased brittleness. Finally, yet importantly, the presence of some intact microballoons in the post-mortem fracture analysis indicates that the filler material has generally survived the fabrication process.

The results presented herein highlight the potential roles of combining syntactic foams and cell density gradation in lightweight hexagonal honeycombs. Notably, the density gradation in syntactic foam structures can be achieved by varying the microballoon volume fraction and the microballoon effective density, as discussed in the pioneering work of Gupta [55]. Simultaneous optimization of load-bearing and energy absorption capacities can be achieved more effectively by considering the interplay between the aforementioned variables, *i.e.*, microballoons effective density and volume fraction, as well as cell wall thickness. While only two out of these three variables were considered in this work, true optimization of honeycombs with syntactic foam cell walls could be the ultimate goal of future research on the topic.

4. Summary

The load-bearing and energy absorption responses of hexagonal honeycomb structures with syntactic cell walls were investigated. Cell wall thickness, cell density gradation, and volume fraction of the microballoon fillers were varied to examine their individual and collective contributions to the mechanical behavior of the structures. The incorporation of microballoons in the cell walls can lead to improved mechanical energy absorption at the expense of overall strength. In addition, the energy absorption efficiency can be enhanced with the proposed architected structures compared to neat epoxy honeycombs. Spatial gradation of the cell wall thickness was leveraged to optimally tune structural stiffness, densification strain, and relative density. Mesoscale digital image correlation analyses revealed the mechanisms of strain concentration in the cell walls. Postmortem fracture surface observations further revealed the development of brittle fracture in cell walls as the primary failure mode in the structure. A notable limitation of the examined structures was found to be their susceptibility to the aforementioned brittle and semi-brittle fracture that initiated from the vicinity of the cell hinges due to strain accumulation. Nevertheless, the architected structures presented in this work were shown to have the potential to offer tunable mechanical performance with low structural density.

CRediT authorship contribution statement

Nicholas Pagliocca: Methodology, Investigation, Formal analysis, Writing – original draft. **George Youssef:** Conceptualization, Writing – review & editing, Funding acquisition. **Behrad Koohbor:** Conceptualization, Supervision, Writing – review & editing, Funding acquisition.

Declaration of Competing Interest

The authors declare that they have no known competing financial interests or personal relationships that could have appeared to influence the work reported in this paper.

Acknowledgements

This material is based upon work supported by the National Science Foundation under Grant No. 2035660 (B.K.) and Grant No. 2035663 (G. Y.). B.K. acknowledges the financial support from Advanced Materials and Manufacturing Institute (AMMI) at Rowan University. We gratefully acknowledge Prof. Wei Xue of Rowan University for his assistance with SEM imaging.

Data Availability

Data will be made available upon request.

Appendix A. Supplementary material

Supplementary data to this article can be found online at https://doi.org/10.1016/j.compstruct.2022.115866.

References

[1] Qin R, Zhou J, Chen B. crashworthiness design and multiobjective optimization for hexagon honeycomb structure with functionally graded thickness. Adv Mater Sci and Engr 2019;2019:1–13.
[2] de Jonge C, Kolken H, Zadpoor A. Non-auxetic mechanical metamaterials. Non-Auxetic Mechan Metamater Mater 2019;12(4):635.
[3] Florijn B, Coulais C, van Hecke M. Programmable mechanical metamaterials. Program Mechan Metamater Phys Rev Lett 2014;113(17):175503.
[4] Cho J, Choi H, Lee S, Cho C, Han M. Experimental study of the impact characteristics of sandwich composites with aluminum honeycomb cores. Int J Automot Technology 2013;14(3):415–21.
[5] Diel S, Huber O, Saage H, Steinmann P, Winter W. Mechanical behavior of a cellular composite under quasi-static, static, and cyclic compression loading. J Mater Sci 2012;47(15):5635–45.
[6] Duncan O, Shepherd T, Moroney C, Foster L, Venkatraman P, Winwood K, et al. Review of auxetic materials for sports applications: expanding options in comfort and protection. Appl Sci 2018;8(6):941.
[7] Yin S, Guo W, Wang H, Huang Y, Yang R, Hu Z, et al. Strong and tough bioinspired additive-manufactured dual-phase mechanical metamaterial composites. J Mech and Phys of Solids 2021;149:104341.
[8] Koohbor B, Blourchian A, Uddin K, Youssef G. Characterization of energy absorption and strain rate sensitivity of a novel elastomeric polyurea foam. Adv Engr Mater 2021;23(1):2000797.
[9] Koohbor B, Ravindran S, Kidane A. In situ deformation characterization of density-graded foams in quasi-static and impact loading conditions. Int J Impact Engr 2021;150:103820.
[10] Gupta N, Zeltmann S, Shunmugasamy V, Pinisetty D. Applications of polymer matrix syntactic foams. JOM 2014;66(2):245–54.
[11] Qiao P, Wang J. Mechanics of composite sinusoidal honeycomb cores. J Aerosp Engr 2005;18(1):42–50.
[12] Pishvar M, Harne R. Foundations for soft, smart matter by active mechanical metamaterials. Adv Sci 2020;7(18). 2001384-n/a.
[13] Chuang Y, Bao L, Chen P, Lou C, Lin J. Buffering sandwiches made of thermoplastic polyurethane honeycomb grids: manufacturing technique and property evaluations. J Sandw Struct and Mater 2019;21(6):1975–90.
[14] Gibson LJ, Ashby MF. Cellular solids – structure and properties. 2nd Edition. UK: Cambridge University Press; 1999.
[15] Jain V, Johnson R, Ganesh I, Saha B, Mahajan Y. Effect of rubber encapsulation on the comparative mechanical behaviour of ceramic honeycomb and foam. Mater Sci and Engr A 2003;347(1):109–22.
[16] Balawi S, Abot J. The effect of honeycomb relative density on its effective in plane elastic moduli: an experimental study. Compos Struct 2008;84(4):293–9.
[17] Malek S, Gibson L. Effective elastic properties of periodic hexagonal honeycombs. Mech Mater 2015;91(1):226–40.
[18] Huang T, Gong Y, Zhao S. Effective in-plane elastic modulus of a periodic regular hexagonal honeycomb core with thick walls. J Engr Mech 2018;144(2):6017019.
[19] Rahman O, Koohbor B. Optimization of energy absorption performance of polymer honeycombs by density gradation. Compos C 2020;3:100052.
[20] Li K, Gao X, Subhash G. Effects of cell shape and cell wall thickness variations on the elastic properties of two-dimensional cellular solids. Int J Solids and Struct 2005;42(5):1777–95.
[21] Huang J, Gong X, Zhang Q, Scarpa F, Liu Y, Leng J. In-plane mechanics of a novel zero Poisson's ratio honeycomb core. Compos B 2016;89:67–76.
[22] Kolken H, Zadpoor A. Auxetic mechanical metamaterials. RSC Adv 2017;7(9):5111–29.
[23] Gatt R, Mizzi L, Azzopardi J, Azzopardi K, Attard D, Casha A, et al. Hierarchical auxetic mechanical metamaterials. Scientific Rep 2015;5(1):8395.
[24] Sorohan S, Consantinescu D, Sandu M, Sandu A. In-plane homogenization of commercial hexagon honeycombs considering the cell wall curvature and adhesive layer influence. Int J Solids and Struct 2019;156–157:87–106.

[25] Rahman O, Uddin K, Muthulingam J, Youssef G, Shen C, Koohbor B. Density-graded cellular solids: mechanics, fabrication, and applications. Adv Engr Mater 2022;24(1):2100646.
[26] Bates S, Farrow I, Trask R. Compressive behaviour of 3D printed thermoplastic polyurethane honeycombs with graded densities. Mater and Des 2019;162:130–42.
[27] Yu X, Qin Q, Zhang J, He S, Xiang C, Wang M, et al. Crushing and energy absorption of density-graded foam-filled square columns: Experimental and theoretical investigations. Compos Struct 2018;201:423–33.
[28] Ghimire S, Chen J. An extended cohesive damage model study of geometrical ratio effects on failure mechanisms of functionally graded sandwiches with multi-layered cores. Compos Struct 2019;224:110999.
[29] Ghimire S, Chen J. Predicting fracture mechanisms in synthetic foam sandwiches with multi-layered cores using extended cohesive damage model. Eng Fract Mech 2020;223:106719.
[30] Ajdari A, Nayeb-Hashemi H, Vaziri A. Dynamic crushing and energy absorption of regular, irregular and functionally graded cellular structures. Int J Solids and Struct 2011;48(3):506–16.
[31] Zhang X, An L, Ding H. Dynamic crushing behavior and energy absorption of honeycombs with density gradient. J Sandw Struct and Mater 2014;16(2):125–47.
[32] Li S, Liu Z, Shim VPW, Guo Y, Sun Z, Li X, et al. In-plane compression of 3D-printed self-similar hierarchical honeycombs – Static and dynamic analysis. Thin-Walled Struct 2020;157:106990.
[33] Taylor C, Smith C, Miller W, Evans K. Functional grading in hierarchical honeycombs: density specific elastic performance. Compos Struct 2012;94(8):2296–305.
[34] Compton B, Lewis J. 3D-printing of lightweight cellular composites. Adv Mater (Weinheim) 2014;26(34):5930–5.
[35] Gupta N, Woldesenbet E, Mensah P. Compression properties of syntactic foams: effect of cenosphere radius ratio and specimen aspect ratio. Compos A 2004;35(1):103–11.
[36] Movahedi N, Murch GE, Belova IV, Fiedler T. Functionally graded metal syntactic foam: fabrication and mechanical properties. Mater and Des 2019;168:107652.
[37] Gupta N, Ricci W. Comparison of compressive properties of layered syntactic foams having gradient in microballoon volume fraction and wall thickness. Mater Sci and Engr A 2006;427(1):331–42.
[38] Jayavardhan M, Doddamani M. Quasi-static compressive response of compression molded glass microballoon/HDPE syntactic foam. Compos B 2018;149:165–77.
[39] Bardella L, Genna F. Elastic design of syntactic foamed sandwiches obtained by filling of three-dimensional sandwich-fabric panels. Int J Solids Struct 2001;38(2):307–33.
[40] Bardella L, Genna F. On the elastic behavior of syntactic foams. Int J Solids Struct 2001;38(40-41):7235–60.
[41] Gupta N, Ye R, Porfiri M. Comparison of tensile and compressive characteristics of vinyl ester/glass microballoon syntactic foams. Compos B 2010;41(3):236–45.
[42] Afolabi L, Ariff Z, Hashim S, Alomayri T, Mahzan S, Kamarudin K, et al. Syntactic foams formulations, production techniques, and industry applications: a review. J Mater Res and Technology 2020;9(5):10698–718.
[43] Jhaver R, Tippur H. Characterization and modeling of compression behavior of syntactic foam-filled honeycombs. J Reinforced Plast and Compos 2010;29(21):3185–96.
[44] Zhang P, Arceneaux D, Liu Z, Nikaeen P, Khattab A, Li G. A crack healable syntactic foam reinforced by 3D printed healing-agent based honeycomb. Compos B 2018;151:25–34.
[45] Kumar S, Ahmed K. Flexural behavior of stiffened syntactic foam core sandwich composites. J Sandw Struct and Mater 2014;16(2):195–209.
[46] Kumar S, Ahmed K. Effects of ageing on mechanical properties of stiffened syntactic foam core sandwich composites for marine applications. J Cellular Plast 2016;52(5):503–32.
[47] Amith Kumar SJ, Ajith Kumar SJ. Low-velocity impact damage and energy absorption characteristics of stiffened syntactic foam core sandwich composites. Constr Build Mater 2020;246:118412.
[48] Yu Q, Zhao Y, Dong A, Li Y. Mechanical properties of EPS filled syntactic foams prepared by VARTM. Compos B 2018;136:126–34.
[49] Huang R, Li P. Elastic behaviour and failure mechanism in epoxy syntactic foams: the effect of glass microballoon volume fractions. Compos B 2015;78:401–8.
[50] Wouterson EM, Boey FY, Hu X, Wong SC. Specific properties and fracture toughness of syntactic foam: Effect of foam microstructures. Compos Sci Tech 2005;65(11):1840–50.
[51] Avalle M, Belingardi G, Montanini R. Characterization of polymeric structural foams under compressive impact loading by means of energy-absorption diagram. Int J Impact Engr 2001;25(5):455–72.
[52] Ravindran S, Koohbor B, Malchow P, Kidane A. Experimental characterization of compaction wave propagation in cellular polymers. Int J Solids and Struct 2018;139-140:270–82.
[53] Argon AS. The physics of deformation and fracture of polymers. Cambridge University Press; 2013.
[54] Panteghini A, Bardella L. On the compressive strength of glass microballoons-based syntactic foams. Mech Mater 2015;82:63–77.
[55] Gupta N. A functionally graded syntactic foam material for high energy absorption under compression. Mater Lett 2007;61(4-5):979–82.